

Traceable Coplanar Waveguide Calibrations on Fused Silica Substrates up to 110 GHz

Uwe Arz¹, Senior Member, IEEE, Karsten Kuhlmann, Thorsten Dziomba, Gerd Hechtfisher, Senior Member, IEEE, Gia Ngoc Phung, Franz Josef Schmückle, and Wolfgang Heinrich², Fellow, IEEE

Abstract—In this paper, we present a comprehensive uncertainty budget for on-wafer S-parameter measurements of devices on a custom-built fused silica wafer, including instrumentation errors, connector repeatability, and calibration standard uncertainties. All major steps toward achieving traceability with the aid of a multilayer thru-reflect-line calibration for the given measurement scenario are explained. For the first time, it is now possible to compare against each other the relative importance of different sources of uncertainty in on-wafer measurements. Results are shown for three typical devices with varying reflection and transmission characteristics.

Index Terms—Calibration, on-wafer, S-parameters, traceability, uncertainty budget.

I. INTRODUCTION

TRACEABILITY forms the basis for credible measurement results and their associated uncertainties. It is driven by today's global economy needs and usually achieved by an unbroken chain of comparisons, to stated references, typically in the form of standards by National Metrology Institutes (NMIs) or designated laboratories. In coaxial and rectangular waveguide S-parameter measurements, traceability to dimensional measurements has been established for a number of years already, with challenges remaining at higher frequencies due to shrinking connector sizes.

For on-wafer S-parameter measurements, however, a number of additional challenges need to be taken into consideration. Planar devices and calibration standards are fabricated on a multitude of substrate materials in a great variety of technologies, and instead of standardized connectors, nowadays,

Manuscript received September 19, 2018; revised January 16, 2019; accepted March 3, 2019. Date of publication April 18, 2019; date of current version June 4, 2019. This work was supported by the European Metrology Programme through the Innovation and Research (EMPIR) Project 14IND02 Microwave Measurements for Planar Circuits and Components. The EMPIR Program is cofinanced by the participating countries and from the European Union's Horizon 2020 Research and Innovation Program. (Corresponding author: Uwe Arz.)

U. Arz, K. Kuhlmann, and T. Dziomba are with Physikalisch-Technische Bundesanstalt (PTB), 38116 Braunschweig, Germany (e-mail: uwe.arz@ptb.de).

G. Hechtfisher is with Rohde & Schwarz GmbH & Co. KG, 81671 Munich, Germany.

G. N. Phung, F. J. Schmückle, and W. Heinrich are with the Ferdinand-Braun-Institut für Höchstfrequenztechnik, 12489 Berlin, Germany.

Color versions of one or more of the figures in this paper are available online at <http://ieeexplore.ieee.org>.

Digital Object Identifier 10.1109/TMTT.2019.2908857

a number of microwave probes from several vendors are in common use.

In the European Project PlanarCal [1], a major effort is currently undertaken to characterize components and devices for eventual use in high-speed and microwave applications (e.g., wireless communications, automotive radar, and medical sensing) with known measurement uncertainties. To this end, parasitic modes as well as effects occurring at higher frequencies such as radiation, dispersion, and surface roughness have been investigated together with the impact of the probe itself and its neighborhood.

The influence of the neighborhood on coplanar waveguides (CPWs) used as standards for multilayer thru-reflect-line (TRL) calibrations [2] was demonstrated for CPWs on GaAs and Al₂O₃ (alumina) substrates in [3] and [4], respectively. The latter investigation included different probe geometries and suggested measures to suppress the occurrence of substrate modes. In [5], a similar investigation was performed for thin-film microstrip lines. The impact of radiation losses due to multimode propagations on TRL calibrations in the WR10 band was described in [6].

All the investigations confirmed that the measurement result depends on the environment as well as on the specific combination of substrate material, planar waveguide type, and probes. Only for such fully specified combinations, and only when single-mode propagation is ensured, reliable uncertainties for on-wafer S-parameters can be stated.

Recently, traceability has been demonstrated for devices built in membrane technology [7]. The corresponding uncertainty budget comprised instrumentation errors (without cables), connector repeatability, and calibration standard uncertainties. The task in [7] was somewhat simplified by the fact that in membrane technology devices, the influence of the thin supporting dielectric material is significantly reduced (see [8]) in comparison to the influence of several-hundred-micrometers-thick substrates that are conventionally used.

In this paper, we focus on planar devices on a custom-built fused silica substrate, where the influence of the substrate material needs to be taken fully into account. This necessitates the wideband extraction of the complex permittivity in the entire frequency range under consideration. To achieve the highest precision in the dimensional characterization of the calibration standards, we used atomic force microscopy (AFM).

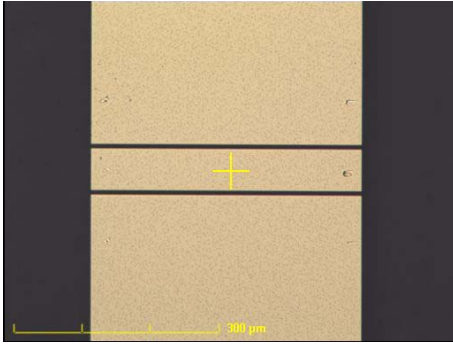


Fig. 1. Thru calibration standard fabricated on fused silica substrate.

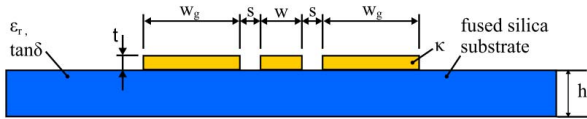


Fig. 2. Cross section of CPW (dimensions not to scale).

In the following sections, we describe the layout and technology used for the custom-built wafer, show simulation and modeling results, introduce the measurement setup used, describe the VNA measurement model and the characterization of the input quantities including AFM, and give an overview of typical results and uncertainty budgets achieved for devices with varying reflection and transmission characteristics.

II. LAYOUT AND TECHNOLOGY

In [9], test structures on an Al_2O_3 substrate were described, which were specifically designed for the investigation of parasitic mode effects and their correction in CPW calibrations. The layout of our custom-built fused silica wafer used the layout of the wafer in [9] as a basis, with modifications regarding the addition of mismatched lines and offset reflects as well as changes in the cross-sectional dimensions to achieve a characteristic impedance of the CPW near 50Ω .

The calibration structures were fabricated on deep UV, fluorescence-free-grade fused silica wafers. In the first step, a thin film of NiCr is sputtered as a resistor layer. The resistor geometry is then formed by optical lithography and wet chemical etching. After the deposition of the resistors, a thin adhesive layer of titanium-tungsten (TiW) and a 500-nm gold layer (Au) is sputtered on the top side of the wafer. The conductor geometry is then formed by optical lithography and wet chemical etching processes. The electrical values of the NiCr resistors are adjusted by laser trimming.

Fig. 1 shows the top view of a 400- μm -long CPW serving as thru calibration standard for a multiline TRL calibration [2]. Scratch marks of the 100- μm -pitch microwave probes used for the measurements can be detected on both sides of the CPW.

III. CPW MODELING AND SIMULATIONS

Fig. 2 shows the cross section of a CPW resulting from the technology described in the previous section together with

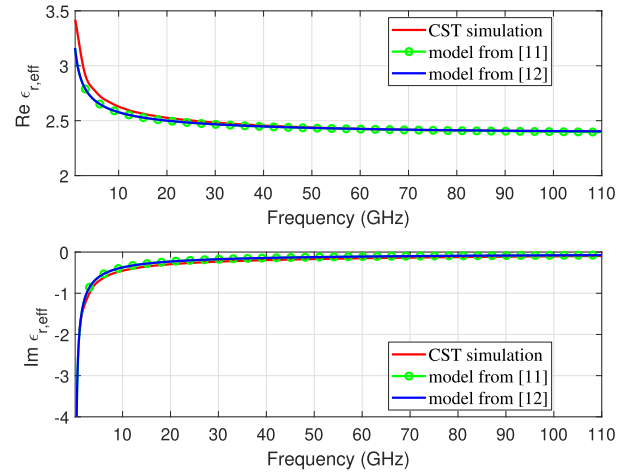


Fig. 3. Real and imaginary parts of $\epsilon_{r,\text{eff}}$ before characterization.

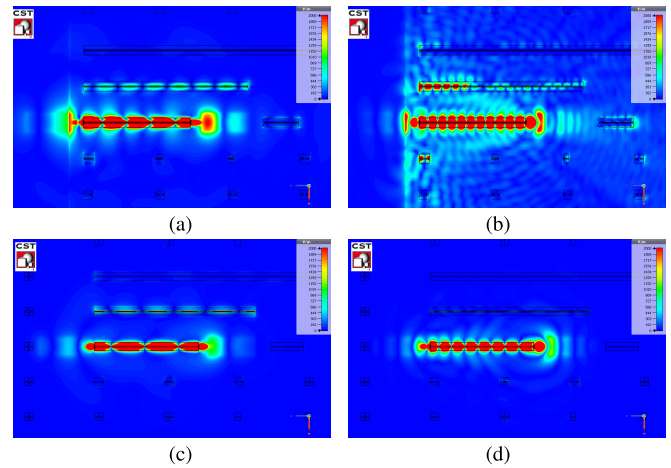


Fig. 4. Simulation of neighborhood effects on 7.4-mm-long CPW lines built on different substrates (color-coded plots of electric field magnitude). (a) Al_2O_3 substrate at 40 GHz. (b) Al_2O_3 substrate at 100 GHz. (c) SiO_2 substrate at 40 GHz. (d) SiO_2 substrate at 100 GHz.

its geometrical and material parameters. In order to validate the model for this design, electromagnetic (EM) simulations of the complete wafer with all the details are performed with CST Microwave Studio [10]. In the simulations, the wafer is placed on a ceramic chuck ($\epsilon_r = 6.5$) with a thickness of 2000 μm extended with open boundary condition, which emulates a realistic measurement environment (thickness of chuck approx. 8 mm). For the excitation, a detailed probe model, which was already implemented in [3]–[5], is used.

The real and imaginary parts of the effective permittivity are calculated through a calibration procedure using the simulated raw data of the calibration set (see Fig. 3). The results are then compared to the analytical model in [11] and its extended version [12] which considers modal dispersion and radiation losses. What can be observed is that there is a relatively good agreement between the CST simulation and the analytical results, which proves the validity of the model. The results also predict a low radiation and dispersion behavior.

The field plots shown in Fig. 4 reveal that the present fused silica substrate shows less coupling and radiation effects to adjacent structures in comparison to the alumina substrate

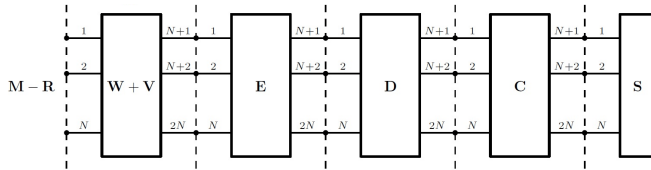


Fig. 5. VNA measurement model (from [14]).

(for which the impact of neighborhood was already investigated in [4]). Due to the mismatch of the dielectric constants for the chuck material ($\epsilon_r = 6.5$) and Al_2O_3 ($\epsilon_r = 9.7$), substrate modes can be excited (at $f = 100$ GHz), which lead to emphasized radiation effects and, in turn, to parasitic coupling to the neighboring structures. Fused silica substrate, on the other hand, has a lower dielectric constant of $\epsilon_r = 3.78$ compared to the chuck material ($\epsilon_r = 6.5$).

Hence, for the simulated case with an open boundary at the bottom, this type of three-layer structure does not support any substrate modes which shows up in a reduced coupling behavior for the fused silica substrate. One should note that in reality during measurements, the whole stackup (fused silica/ceramic configuration) is placed on a metal chuck forming the GND. In this case, slab modes in the ceramic chuck and a “microstrip-like” mode without cutoff frequency can be excited. But due to the large thickness of the ceramic chuck in comparison to the CPW dimensions, the field overlap between the slab modes and the CPW mode is very small and, thus, coupling vanishes. Similarly, the effect of the “microstrip-like” mode is governed by the ratio between the total CPW width and the thickness of the substrate plus the ceramic support, which is below 0.07. Hence, the effect of substrate and “microstrip-like” modes can be neglected and the case of an open boundary at the bottom is an excellent approximation. This has been verified by simulations. Overall, the in-depth analysis through EM simulations not only assesses the validity of the model but also shows the potentials of the fused silica substrate for establishing traceability of on-wafer measurements.

IV. VNA MEASUREMENT MODEL AND CALIBRATION

The evaluation of S-parameter uncertainty depends on a number of factors such as instrumentation errors, cable, and connector repeatability, standard uncertainties, the calibration algorithm chosen, and the DUT itself. This complicated task is greatly simplified with modern software tools such as [13] or [14], which have been recently compared in [15] and [16]. In our approach, we established a comprehensive uncertainty budget for the entire measurement process using the linear uncertainty propagation library *Metas.UncLib* [17], which is based on the automatic differentiation techniques in [18].

For the calculation of corrected S-parameters from the measured raw data and the propagation of measurement as well as calibration standard uncertainties to the final results, the VNA measurement model described in [14] and [19] has been applied.

Fig. 5 shows a block diagram of the general N -port measurement model (in our case $N = 2$). The symbols denote the



Fig. 6. PTB on-wafer measurement setup.

raw data measured by the VNA (M), the noise/linearity influences (R), the switch terms (W), the drift of the switch terms (V), the calibration error terms (E), the drift of the calibration error terms (D), the cable stability/connector repeatability and DUT uncertainty influences (C), and the error corrected data (or calibration kit standard definitions) (S), respectively. The vertical dashed lines represent the reference planes of the S-parameters of the cascaded model sections.

The error terms of the underlying seven-term error model were calculated with the multiline TRL calibration algorithm described in [2] and [20]. Nine lines with CPW lengths between 400 and 20400 μm were used, assuming a length uncertainty of 10 μm and a uniform probability density function (PDF).

Since the multiline TRL method, as a self-calibration technique, does not allow for a straightforward propagation of calibration standard uncertainties, the influence of these uncertainties was calculated using the recursive approaches described in [21] and [22]. In [7], these influences were estimated with the Microwave Uncertainty Framework developed at NIST [13].

V. ON-WAFER MEASUREMENT SETUP

Fig. 6 shows the on-wafer measurement setup used at Physikalisch-Technische Bundesanstalt (PTB). Measurements were performed on a ceramic chuck utilizing an Anritsu VectorStar VNA with millimeter-wave (mm-wave) extension modules for frequencies up to 125 GHz, connected to GGB ground-signal-ground microwave probes with 100- μm pitch. To enable automated multiline TRL calibrations, a semi-automated wafer prober (Süss PA 200) with motorized x/y -positioner on the right-hand side was used. Up to 30 GHz, the VNA base unit was used, and above 30 GHz, the mm-wave extensions. This leads to different VNA uncertainty contributions over frequency, as can be seen in Section VI.

VI. CHARACTERIZATION OF INPUT QUANTITIES

In the following, the input quantities relevant for the measurement process are listed with their respective values and/or uncertainties (coverage factor is $k = 2$ unless

TABLE I
UNCERTAINTIES DUE TO NOISE ($K = 1$)

Frequency (GHz)	Noise Floor (dB)	Trace Noise Mag (dB rms)	Trace Noise Phase (deg rms)
0	-110	0.004	0.03
30	-120	0.003	0.04
30.001	-100	0.003	0.02
55	-100	0.002	0.01
55.001	-115	0.001	0.01
80	-120	0.001	0.01
80.001	-115	0.002	0.05
120	-100	0.004	0.03

indicated otherwise). They are typical for the on-wafer measurement setup used at PTB for frequencies up to 120 GHz. All results were obtained and verified through repeated measurements.

A. VNA Characterization

1) *Noise Floor/Trace Noise*: The VNA noise characterization was performed following the procedures outlined in [19, Annex G.1]. Both ports of an uncalibrated VNA were terminated with high reflect standards (open or short). Here, coaxial shorts were used. The S-parameters were measured repeatedly (several hundred times). This was done frequency-point-by-frequency-point in order to reduce drift influences. Table I shows the noise floor and trace noise uncertainties of the VNA used in this paper.

2) *Linearity*: The VNA uncertainty due to nonlinear receiver behavior is usually determined by measuring calibrated step attenuators over a large attenuation range (>60 dB). The detailed procedure is given in [19, Annex G.2]. Alternatively, the data sheet value of the VNA manufacturer can be applied though overestimation is possible. The frequency dependence is generally weak, unless compression effects are present. To start with, the source power level should be reduced such that compression effects are avoided. Here, the uncertainty in linearity was estimated to the values of 0.01 dB for the magnitude and 0.066° for the phase over the complete magnitude and frequency range.

3) *Error Term Drift*: The VNA uncertainty due to the error term drift was determined by measuring a calibrated coaxial through connection over 24 h and is given in Table II. The detailed procedure is given in [19, Annex G.3]. The directivity, match, and switch term drift are related to the reflection coefficient drift of the thru measurements. The error term drift related to transmission is based on the transmission coefficient drift of the thru measurements. Alternatively, an electronic calibration unit (ECU) can be applied to monitor the individual error terms directly over time, assuming that the ECU drift is smaller than the VNA drift, which is usually the case. Table II shows the drift uncertainties of the VNA error terms.

B. Cable Movement

The 1-mm cables connecting to the GSG probes were fixed during the measurements. The movement of the cables leading to the mm-wave extensions essentially affects only

TABLE II
UNCERTAINTIES DUE TO ERROR TERM DRIFT

Frequency (GHz)	Switch Term (dB)	Directivity (dB)	Tracking		Symmetry		Match (dB)
			Mag (dB)	Phase (deg)	Mag (dB)	Phase (deg)	
0	-35	-35	0.07	0.6	0.025	0.4	-35
10	-35	-35	0.07	0.6	0.025	0.4	-35
10.001	-35	-35	0.03	1.0	0.01	0.2	-35
20	-35	-35	0.03	1.0	0.01	0.2	-35
20.001	-35	-35	0.06	1.4	0.03	0.2	-35
30	-35	-35	0.06	1.4	0.03	0.2	-35
30.001	-50	-50	0.03	0.8	0.01	0.3	-50
120	-50	-50	0.03	0.8	0.01	1.1	-50

TABLE III
UNCERTAINTIES DUE TO CABLE MOVEMENT

Frequency (GHz)	Reflection Stability (dB)	Transmission Stability Mag (dB)	Transmission Stability Phase (deg)
0	-50	0.05	0.1
30	-50	0.05	0.4
30.001	-60	0.01	0.1
120	-60	0.01	0.1

measurements up to 30 GHz and was neglected in [7]. Here, however, the cable effects were determined as described in [19, Annex G.4]. The cables attached to the first port were not moved. The cables and the mm-wave extension at port two were repeatedly (> ten times) moved between two points that are representative for the largest movements for typical DUTs. Calibrated measurements were recorded at each point while the mm-wave extension was terminated with a coaxial short and a coaxial match, respectively. The cable reflection stability is determined by the load measurements, the transmission stability by the short measurements. The results are given in Table III.

C. Connection Repeatability

The repeatability of coaxial connectors is usually determined by repeated connection and measurement of a stable termination [19, Annex G.5]. For the on-wafer scenario, the same approach is applied. After a VNA calibration, the probe was repeatedly (> eight times) connected to a stable termination (here, on-wafer open standard). During this test, only the chuck was moved, not the cables. For the given setup, a repeatability of better than -60 dB was obtained for the complete frequency range, which is shown in Fig. 7.

D. DUT Uncertainty/Crosstalk

In [9], a crosstalk correction method was demonstrated to significantly improve measurements of an attenuator built on an alumina substrate. Fig. 8 shows the comparison of the measurements of attenuators built on a similar alumina substrate and on the fused silica substrate under investigation in this paper, respectively, both before applying the crosstalk correction in [9]. While the multiline-TRL-corrected transmission coefficient magnitude measurement of the attenuator on alumina shows a pronounced increase for higher frequencies, the measurement of the fused silica attenuator remains almost

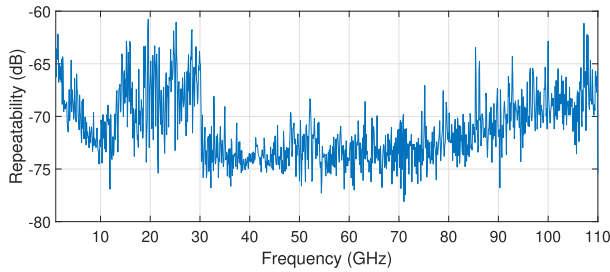


Fig. 7. On-wafer measurement connection repeatability (log magnitude). Repeatability is defined here as the maximum of the differences in real and imaginary parts between all reflection measurements.

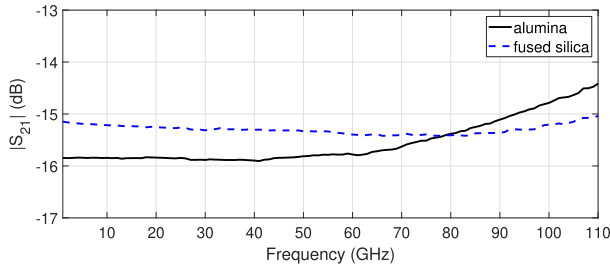


Fig. 8. Measured transmission of attenuator device on different substrates.

TABLE IV
TRANSMISSION UNCERTAINTIES DUE TO CROSSTALK (IN dB)

Reflection Mag (lin. mag.)	Frequency (GHz)			
	0	20	50	120
0.0	-60	-55	-50	-45
0.2	-60	-55	-50	-45
0.8	-60	-40	-35	-20
1.0	-60	-40	-35	-20

constant over the entire frequency range. We, therefore, chose not to perform the crosstalk correction of [9].

Instead, the effect of crosstalk has been modeled as uncertainty contribution with the DUT uncertainty approximation described in [14]. This approximation is based on the observation that, depending on the frequency as well as on the reflection coefficient magnitude of the measured device, significant levels of transmission can be measured. The DUT uncertainty approximation does not aim to replace crosstalk correction methods such as in [9] but rather provide an estimate of the measurement uncertainty introduced by the crosstalk energy between adjacent device ports.

The values given in Table IV were estimated as upper limits from measurements of the transmission coefficient magnitude between the two ports of high-reflect (i.e., offset-open and offset-short) and lumped-load structures on the fused silica substrate. Currently, crosstalk effects on reflections are neglected. The DUT uncertainty approximation is clearly only a first attempt to describe the uncertainties caused by crosstalk, and there is more work required in this area.

E. Dielectric Material Characterization

Three different sources of information were considered for determining the dielectric material properties of the fused silica substrate in the frequency range up to 110 GHz. At low frequencies, manufacturer specifications were given for

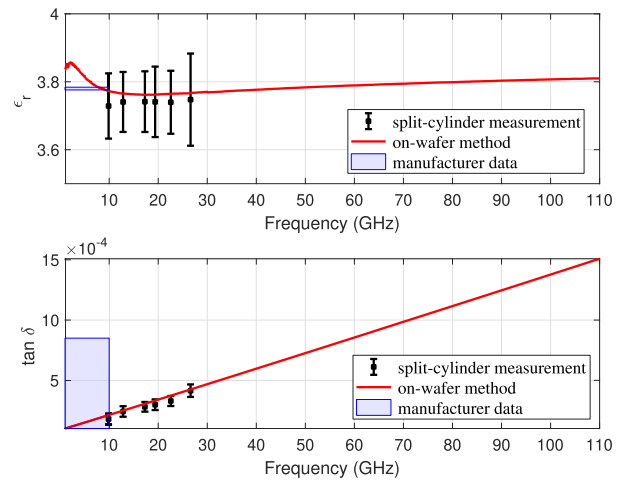


Fig. 9. Dielectric material characterization.

both ϵ_r and $\tan \delta$. For intermediate frequencies in the range 10–26 GHz, a commercially available split-cylinder resonator [23] was used at PTB to determine the relative permittivity and the loss tangent. In addition, the on-wafer methods in [24]–[26] were used to cover the entire frequency range from 1 to 110 GHz.

The results including the standard uncertainties of the split-cylinder measurements are shown in Fig. 9. For both ϵ_r and $\tan \delta$, the values extracted with the on-wafer methods agree well with the split-cylinder resonator measurements and their uncertainties in the frequency range where the split-cylinder method is applicable. While the relative permittivity is nearly constant in the entire frequency range, the loss tangent increases linearly with frequency. In [23], a similar linear frequency dependence for $\tan \delta$ was observed for a different type of fused silica material for frequencies up to 50 GHz when using split-cylinder resonators built for TE₀₁₁ resonant modes at 10 and 35 GHz, respectively.

In contrast to the split-cylinder methods, where the uncertainties are traceable to dimensional measurements of the cylindrical cavity, the uncertainties of the on-wafer methods have not been fully established yet. Therefore, conservative estimates are used for ϵ_r and $\tan \delta$ based on the results shown in Fig. 9. For both quantities, a uniform PDF is assumed, which means the values of all input quantities are assumed to lie within an interval $[a, b]$ with a lower limit a and an upper limit b . The half-widths of this interval were determined from Fig. 9 as $(b - a)/2$. The resulting values used for the entire frequency range under consideration are $\epsilon_r = 3.78 \pm 0.15$ and $\tan \delta = (8 \pm 7) \cdot 10^{-4}$.

F. Dimensional Characterization of Calibration Standards by AFM

High-resolution dimensional measurements were performed with the Nanostation II noncontact AFM (by SIS Surface Imaging Systems, Germany; now known as H8 Neos by Bruker). This AFM has the advantage that the scanner for the lateral axes is physically decoupled from the vertical scanner, which avoids any major disturbing flatness deviations.

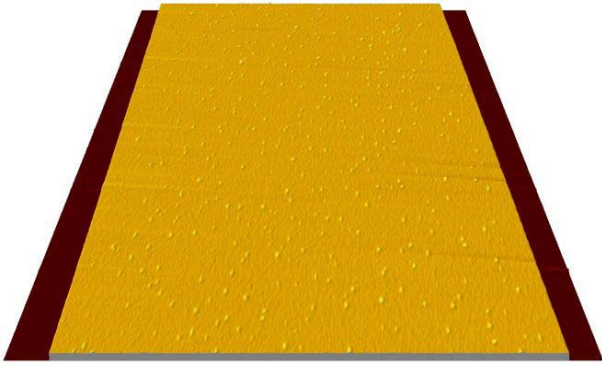


Fig. 10. 3-D view of $74 \mu\text{m} \times 93 \mu\text{m} \times 0.78 \mu\text{m}$ (z shown $3\times$ enlarged).

It is a system of category B according to ISO 11952 and VDI/VDE 2656-1, i.e., it is equipped with well-calibrated sensors along all three spatial axes: capacitive sensors with closed-loop position control in x and y , and a highly linear strain gauge sensor in z . The system is operated under very stable conditions in the PTB cleanroom center and regularly calibrated.

For most investigations reported here, SSS tips (“Super-SharpSilicon” tips by Nanosensors, Germany) with an apex radius of some very few nanometers have been used; at most structure groups, both a large AFM image of $100 \mu\text{m} \times 108 \mu\text{m}$ to measure the top width between the pairs of CPW grooves as well as two smaller images of $27 \mu\text{m} \times 108 \mu\text{m}$ across each of the grooves to determine their shape (width and edge slope including line-edge roughness) have been recorded. As the sample shows slight nanoscopic contamination, amplitude control needs to be set to rather robust values, which, in turn, means a rather strong tip wear. To counter this effect, most images have been recorded with 64 scanlines only (with 1024 data points each), i.e., the cross sections are probed at high pixel resolution, while properties along the bar (such as the line-edge roughness) are, thus, determined at a lower resolution. Some few images were recorded at full resolution of 1024×1024 data points, e.g., for roughness analysis (Fig. 10). While the scan speed was generally chosen low with $10\text{--}20 \mu\text{m/s}$, some few extra-slow scans with $2 \mu\text{m/s}$ were performed that no longer show any discrepancy between forward and backward profiles (trace-retrace) and thereby serve as reference for the other measurements. Image analysis was mainly accomplished with the software package SPIP (Scanning Probe Image Processor, by Image Metrology, Denmark), version 6.

According to VDI/VDE 2656-1 and ISO 11952, step height analysis in AFM images is either done by a method relying on the histogram of height values measured or in analogy to ISO 5436 once developed for profilometers. The latter takes the central section of a line w_m and two reference sections of length w_s to the left and right of it, in the adjacent grooves, into account (Fig. 11), deliberately omitting the edge transition that is often subject to contamination, curvature at the edges or control errors. For structures like here, the section lengths need to be carefully adjusted to match with the cross section. The analysis is based on the fit of a pair of parallel lines through

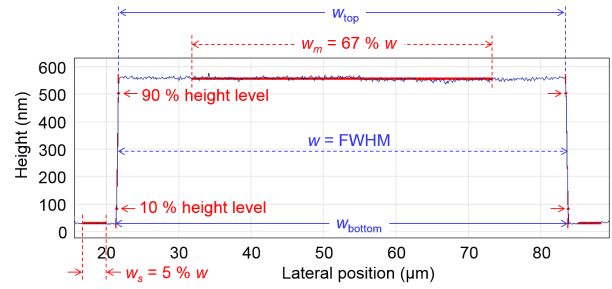


Fig. 11. Analysis of a measured profile. Section lengths criteria: w_m and w_s , determined top linewidth w_{top} and bottom linewidth w_{bottom} .

these three sections: through the central section of length w_m for the upper fit line and the two sections each of length w_s for the lower fit line. The (vertical) distance between these lines equals the step height t . Furthermore, this analysis can be expanded to slopes and widths: The 10% to 90% height levels of the edge transitions are taken as basis to fit a slope line; its slope is the slope angle of the edge. The intersections of these slope lines with the previously fit pair of parallel lines define the end points of the widths (top linewidth w_{top} , bottom linewidth w_{bottom}) of lines or, alternatively, grooves. This analysis is typically done profilewise (i.e., scanline by scanline), thus yielding statistics on the parameters’ variation across the AFM image, followed by averaging over all valid results of the individual scanlines. Contamination occasionally requires postprocessing of the automatically calculated results, as, e.g., a contamination particle might be misinterpreted as an elevation.

The depth of the CPW grooves could be determined to 534.5 nm with an expanded uncertainty $U(k=2)$, i.e., approximately 95% coverage interval, in the range of 2.5 nm ; the main uncertainty contribution is sample inhomogeneity and contamination. The width w of the material between the CPW grooves turned out to be $62.0 \mu\text{m}$ with $U(k=2) = 0.6 \mu\text{m}$, whereas the widths of the grooves s could be determined with $U(k=2) = 0.2 \mu\text{m}$; the main contribution to the uncertainty in these widths measurement is the tip shape. The edge slopes of these grooves varied from 54° to 67° . The roughness on top is about $S_q = 4 \text{ nm}$ [root-mean-square (rms) roughness] for a measurement area of $60 \mu\text{m} \times 60 \mu\text{m}$ at 600×600 data points (leveled, without spatial filters, obvious contamination particles excluded from roughness analysis).

VII. MEASUREMENT-MODEL COMPARISON

Fig. 12 shows the propagation constant $\gamma = \alpha + j\beta$ of the fabricated CPW lines calculated with both the model in [11] and the extended model in [12] including the uncertainties from the dielectric material and dimensional characterization (dashed lines). Both model values virtually coincide, which confirms the absence of modal dispersion in the frequency range under investigation. Also shown are the values of the propagation constant measured with multilines TRL. They agree well with the model values within the uncertainty bounds determined by the input quantity characterization results.

Fig. 13 shows the comparison of the measured and model-based values of reflection and transmission S-parameters of

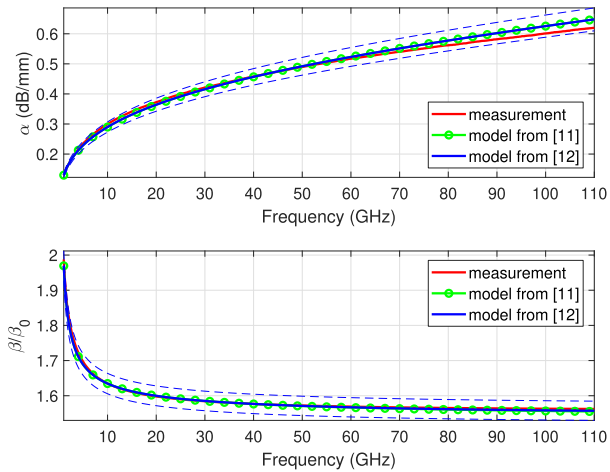


Fig. 12. Comparison between measured (red) and modeled (blue and green) attenuation α and phase constant β , normalized to the free-space value β_0 .

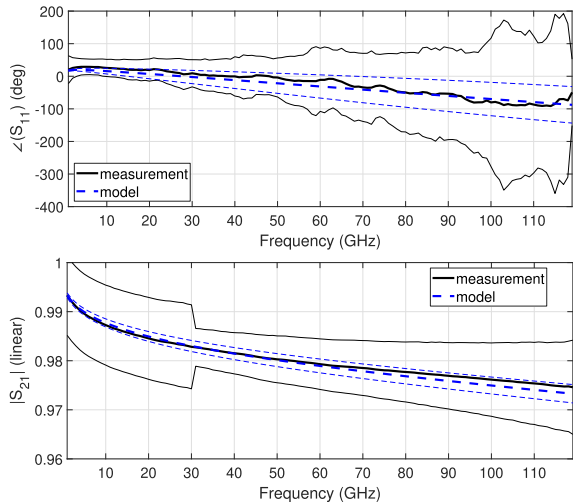


Fig. 13. Comparison between measured (solid) and modeled (dashed) reflection and transmission S-parameters of a 400- μm -long matched line.

a 400- μm -long matched line. Thick lines indicate nominal values, thin lines indicate the expanded uncertainty intervals at a coverage probability of 95% ($k = 2$). The S-parameters are normalized to 50 Ω . The expanded uncertainty intervals calculated from the VNA model shown in Fig. 5 are in very good agreement with the line model values in the frequency range from 1 to 110 GHz.

VIII. DUT UNCERTAINTY RESULTS

In the following, results for three typical devices are shown, covering a large portion of the impedance range measurable by a VNA: a nominally 15-dB matched attenuator (termed “attenuator”), a 7065- μm -long mismatched line (termed “mismatch”), and a two-port open (high-reflect device, termed “open”).

Fig. 14 shows the magnitude of the measured transmission S-parameter S_{21} for the three devices including their expanded uncertainties at a coverage probability of 95% ($k = 2$). All S-parameters were normalized to the system reference impedance of 50 Ω .

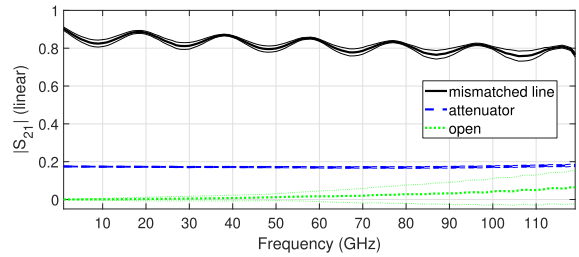


Fig. 14. Measured transmission including expanded uncertainties.

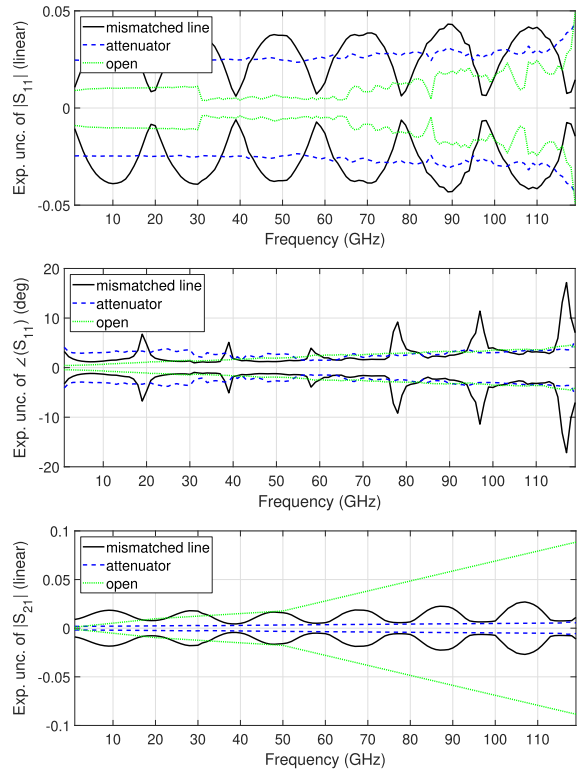


Fig. 15. Lower and upper limits of expanded uncertainty intervals at a coverage probability of 95% ($k = 2$).

To this end, the characteristic impedance Z_0 of the line standards was determined from the measured propagation constant γ using the low-loss approximation of constant capacitance per unit length C and negligible conductance per unit length G described in [27], i.e., $Z_0 = \gamma / (j\omega C + G) \approx \gamma / (j\omega C)$.

The capacitance per unit length C is treated as independent uncertain quantity in our current budget calculations, as it can be determined either from measurement [28] or from model calculations. Here, we used the models in [11] and [12], which both gave nearly identical results. Surface roughness effects are negligible because of the low value of S_q .

A. Expanded Uncertainties and Measurement Spread

Fig. 15 shows the expanded uncertainty intervals at a coverage probability of 95% ($k = 2$) of reflection and transmission S-parameters for all three devices considered.

As the custom-built fused silica wafer did not contain multiple copies of the same device in different locations, three repeat measurements of the same device were conducted on

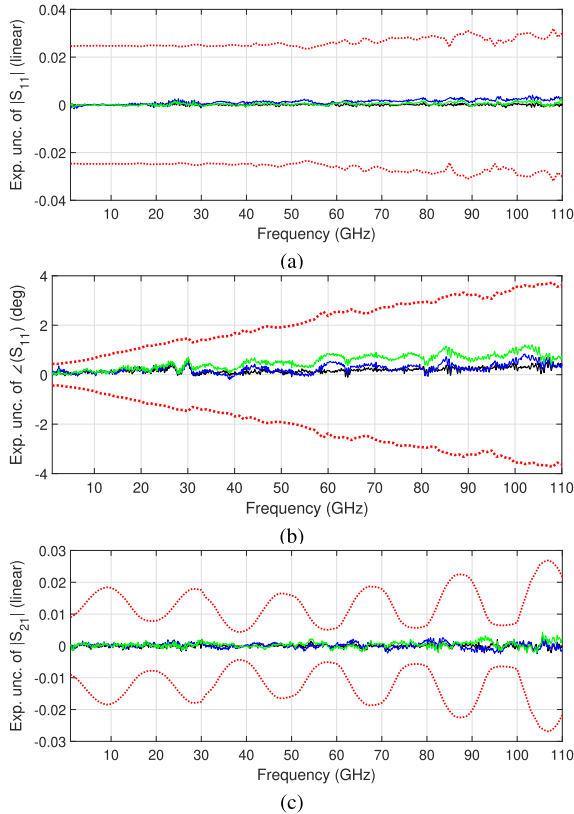


Fig. 16. Spread of repeat DUT measurements (solid lines) versus lower and upper limits of expanded uncertainty intervals (dashed lines). The three repeat measurements were normalized to the first DUT measurements taken. (a) Attenuator. (b) Open. (c) Mismatched line.

different days using the same measurement equipment. The spread of the corrected DUT measurements falls well within the expanded uncertainties predicted by our budget, as shown exemplarily in Fig. 16.

B. Uncertainty Budgets

For the three selected devices, exemplary uncertainty budgets for selected measurement quantities are shown in Fig. 17. In most cases shown, the budget is dominated by the calibration standard uncertainties (red curve), which include the uncertainties of the renormalization step to 50Ω . Within the calibration standard uncertainties, the uncertainties in C and in ϵ_r are usually the dominant factor. The latter is also a consequence of the rather conservative uncertainty estimation for ϵ_r in Section VI-E. However, for certain constellations, also the uncertainties in the line lengths can be the biggest contributor, e.g., in the case of $\angle S_{21}$ of the mismatched line.

For the open device, cable stability becomes dominant in the budget of $|S_{11}|$ up to 30 GHz. For all three devices and the quantities shown, VNA drift has a significant impact at low frequencies up to 30 GHz, which is a direct consequence of the VNA architecture used. In the magnitude and phase of S_{21} , the influence of the DUT uncertainty approximation becomes significant at increasing frequencies for medium-to high-reflect devices. This becomes also evident from the mismatch and open results shown in Figs. 14 and 15 (bottom graph).

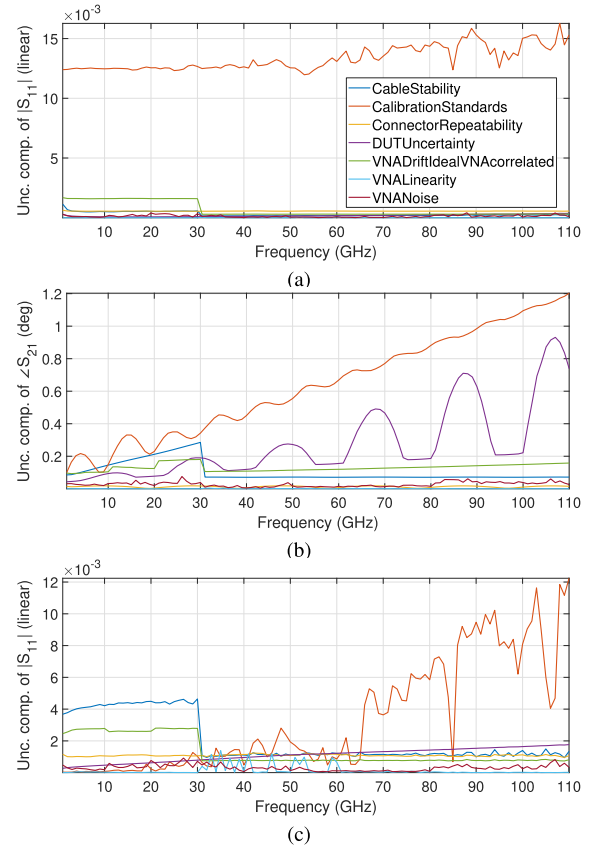


Fig. 17. Uncertainty budget components for three devices over frequency. (a) $|S_{11}|$ of attenuator. (b) $\angle S_{21}$ of mismatched line. (c) $|S_{11}|$ of open.

In summary, the graphs shown in Fig. 17 together with corresponding graphs of subbudgets (e.g., for calibration standard uncertainties, not shown here) allow for a better understanding of the impact of different input quantities. This can provide immediate understanding which quantities one needs to focus on in order to achieve lower uncertainties.

IX. CONCLUSION

In this paper, a comprehensive uncertainty budget was demonstrated for multiline-TRL-corrected on-wafer S-parameter measurements on a conventional thin-film substrate. The budget includes instrumentation errors such as VNA noise, linearity, drift, cable stability, and also connection repeatability, uncertainties from crosstalk between the measurement ports, and calibration standard uncertainties. Some of the uncertainties shown here can be significantly reduced by improving on the measurements of the wideband frequency-dependent material properties, which is a subject of future research. The methodology presented in this paper can be applied to other configurations of measurement hardware, substrate materials, and probes, as long as single-mode propagation is ensured.

ACKNOWLEDGMENT

The authors would like to thank T. Probst, S. Zinal, D. Schubert, and D. Schulz from PTB for their expert technical assistance. They would also like to thank D. F. Williams from NIST for providing the layout of the alumina wafer used in [9].

REFERENCES

- [1] European Metrology Programme for Innovation and Research JRP Number 14IND02. *Microwave Measurements for Planar Circuits and Components*. Accessed: Apr. 12, 2019. [Online]. Available: <https://planarcal.ptb.de>
- [2] R. B. Marks, "A multiline method of network analyzer calibration," *IEEE Trans. Microw. Theory Techn.*, vol. 39, no. 7, pp. 1205–1215, Jul. 1991.
- [3] F. J. Schmückle, T. Probst, U. Arz, G. N. Phung, R. Doerner, and W. Heinrich, "Mutual interference in calibration line configurations," in *Proc. 89th ARFTG Microw. Meas. Conf.*, Jun. 2017, pp. 1–4.
- [4] G. N. Phung, F. J. Schmückle, R. Doerner, W. Heinrich, T. Probst, and U. Arz, "Effects degrading accuracy of CPW mTRL calibration at W band," in *IEEE/MTT-S Int. Microw. Symp. Dig.*, Jun. 2018, pp. 1296–1299.
- [5] G. N. Phung, F. J. Schmückle, R. Doerner, T. Fritzsche, and W. Heinrich, "Impact of parasitic coupling on multiline TRL calibration," in *Proc. 47th Eur. Microw. Conf.*, Oct. 2017, pp. 835–838.
- [6] M. Spirito, C. D. Martino, and L. Galatro, "On the impact of radiation losses in TRL calibrations," in *Proc. 91st ARFTG Microw. Meas. Conf.*, Jun. 2018, pp. 1–3.
- [7] U. Arz, S. Zinal, T. Probst, G. Hechtfisher, F. J. Schmückle, and W. Heinrich, "Establishing traceability for on-wafer S-parameter measurements of membrane technology devices up to 110 GHz," in *Proc. 90th ARFTG Microw. Meas. Symp.*, Nov. 2017, pp. 1–4.
- [8] U. Arz, M. Rohland, and S. Büttgenbach, "Improving the performance of 110 GHz membrane-based interconnects on silicon: Modeling, measurements, and uncertainty analysis," *IEEE Trans. Compon. Packag. Manuf. Technol.*, vol. 3, no. 11, pp. 1938–1945, Nov. 2013.
- [9] D. F. Williams, F. J. Schmückle, R. Doerner, G. N. Phung, U. Arz, and W. Heinrich, "Crosstalk corrections for coplanar-waveguide scattering-parameter calibrations," *IEEE Trans. Microw. Theory Techn.*, vol. 62, no. 8, pp. 1748–1761, Aug. 2014.
- [10] Microwave Studio(MWS). (2018). *CST—Computer Simulation Technology AG*. [Online]. Available: www.cst.com/products/cstmws
- [11] W. Heinrich, "Quasi-TEM description of MMIC coplanar lines including conductor-loss effects," *IEEE Trans. Microw. Theory Techn.*, vol. 41, no. 1, pp. 45–52, Jan. 1993.
- [12] F. Schnieder, T. Tischler, and W. Heinrich, "Modeling dispersion and radiation characteristics of conductor-backed CPW with finite ground width," *IEEE Trans. Microw. Theory Techn.*, vol. 51, no. 1, pp. 137–143, Jan. 2003.
- [13] D. F. Williams. (2012). *NIST Microwave Uncertainty Framework, Beta Version*. [Online]. Available: www.nist.gov/services-resources/software/wafer-calibration-software
- [14] M. Wollensack and J. Hoffmann. (2017). *METAS VNA Tools II—Math Reference*. [Online]. Available: www.metas.ch
- [15] V. Teppati and A. Ferrero, "A comparison of uncertainty evaluation methods for on-wafer S-parameter measurements," *IEEE Trans. Instrum. Meas.*, vol. 63, no. 4, pp. 935–942, Apr. 2014.
- [16] G. Avolio *et al.*, "Software tools for uncertainty evaluation in VNA measurements: A comparative study," in *Proc. 89th ARFTG Microw. Meas. Conf.*, Jun. 2017, pp. 1–7.
- [17] M. Zeier, J. Hoffmann, and M. Wollensack, "Metas.UncLib—A measurement uncertainty calculator for advanced problems," *Metrologia*, vol. 49, no. 6, p. 809, Nov. 2012.
- [18] B. D. Hall, "Calculating measurement uncertainty using automatic differentiation," *Meas. Sci. Technol.*, vol. 13, no. 4, p. 421, Feb. 2002.
- [19] EURAMET CG-12. (2018). *Guidelines on the Evaluation of Vector Network Analysers (Calibration Guide No. 12 Version 3.0)*. [Online]. Available: www.euramet.org/publications-media-centre/calibration-guidelines
- [20] D. C. DeGroot, J. A. Jargon, and R. B. Marks, "Multiline TRL revealed," in *60th ARFTG Conf. Dig.*, Washington, DC, USA, Dec. 2002, pp. 131–155.
- [21] U. Stumper, "Uncertainty of VNA S-parameter measurement due to nonideal TRL calibration items," *IEEE Trans. Instrum. Meas.*, vol. 54, no. 2, pp. 676–679, Apr. 2005.
- [22] B. Hall, "On evaluating the uncertainty of VNA self-calibration procedures," in *Proc. 1st Workshop Electron. Calibration Units Eur. ANAMET Meeting*, Dec. 2013, pp. 1–16.
- [23] M. D. Janezic, "Nondestructive relative permittivity and loss tangent measurements using a split-cylinder resonator," Ph.D. dissertation, Dept. Elect. Comput. Eng., Univ. Colorado Boulder, Boulder, CO, USA, 2003.
- [24] U. Arz, M. D. Janezic, and W. Heinrich, "Wideband relative permittivity extraction based on CPW phase constant measurements," in *Proc. 77th ARFTG Microw. Meas. Conf.*, Jun. 2011, pp. 1–3.
- [25] U. Arz, "Loss tangent extraction based on equivalent conductivity derived from CPW measurements," in *Proc. IEEE 18th Workshop Signal Power Integr.*, May 2014, pp. 1–4.
- [26] U. Arz, "Microwave substrate loss tangent extraction from coplanar waveguide measurements up to 125 GHz," in *Proc. 83rd ARFTG Microw. Meas. Conf.*, Jun. 2014, pp. 1–3.
- [27] R. B. Marks and D. F. Williams, "Characteristic impedance determination using propagation constant measurement," *IEEE Microw. Guided Wave Lett.*, vol. 1, no. 6, pp. 141–143, Jun. 1991.
- [28] D. F. Williams and R. B. Marks, "Transmission line capacitance measurement," *IEEE Microw. Guided Wave Lett.*, vol. 1, no. 9, pp. 243–245, Sep. 1991.



Uwe Arz (S'97–M'02–SM'09) received the Dipl.-Ing. degree in electrical engineering and the Ph.D. degree (*summa cum laude*) from the University of Hanover, Hannover, Germany, in 1994 and 2001, respectively.



In 2001, he was a Post-Doctoral Research Associate with the National Institute of Standards and Technology, Boulder, CO, USA. In 2002, he joined Physikalisch-Technische Bundesanstalt (PTB), Braunschweig, Germany, where he was involved in the metrology for on-wafer measurements. He is currently the Head of the Working Group Fundamentals of Scattering Parameter Measurements, PTB and also leads the European EMPIR Project PlanarCal as a Coordinator.

Dr. Arz was the recipient of the first ARFTG Microwave Measurement Student Fellowship Award in 1999, the 2003 AHMT Measurement Science Award, three ARFTG Best Poster Awards, two ARFTG Best Paper Awards. He was a co-recipient of the 2011 European Microwave Prize.

Karsten Kuhlmann received the Dipl.-Ing. degree from the Technical University of Braunschweig, Braunschweig, Germany, in 2004, and the Ph.D. degree from the Hamburg University of Technology, Hamburg, Germany, in 2009.

Since 2009, he has been with the National Metrology Institute (NMI), Physikalisch-Technische Bundesanstalt (PTB), Braunschweig, Germany. His current research interests include metrology at microwave and millimeter-wave frequencies and smart antennas.



Thorsten Dziomba received the diploma degree in physics from Wilhelms-Universität Münster, Münster, Germany, where he specialized on scanning probe techniques and surface science in the group of Prof. H. Fuchs.

In 1998, he joined Physikalisch-Technische Bundesanstalt (PTB), Braunschweig, Germany, where he was involved in scanning near-field optical microscopy and dimensional nanometrology. From 2006 to 2017, he was the Coordinator of PTB's Calibration Service by metrological atomic force microscopy and related techniques. He is currently active in several standardization committees on nanotechnology and high-resolution topography measurement techniques. His current research interests include the comparability of different scanning probe and optical techniques in surface roughness measurements on the microscale and nanoscale. He is also a co-pilot of the first international comparisons among National Metrology Institutes (NMIs) in this field.

Mr. Dziomba was a recipient of the Best Young Metrologist of COOMET Prize in 2007.



Gerd Hechtfischer (M'97–SM'10) received the Diploma degree in physics from Technische Universität München, Munich, Germany, in 1994, and the Ph.D. degree in solid-state physics from the University of Erlangen, Erlangen, Germany, in 1997.

He is currently the Head of microwave technology research and development with the Test and Measurement Division, Rohde & Schwarz GmbH & Co. KG, Munich. His current research interests include microwaves, superconductors, and thin-film technology.



Gia Ngoc Phung received the Dipl.-Ing. degree from the Technical University in Berlin, Berlin, Germany, in 2012. She is currently pursuing the Ph.D. degree at the Ferdinand-Braun-Institut, Berlin.

From 2013 to 2015, she joined BIOTRONIK SE & Co. KG, Berlin, where she was involved in the electromagnetic simulation of cardiac devices for development projects. Her current research interests include electromagnetic simulations, mainly in the field of on-wafer measurements, calibration substrates, and microwave packaging.



Franz Josef Schmückle received the Dipl.-Ing.(FH) degree from FH Wiesbaden, Wiesbaden, Germany, in 1980, the Dipl.-Ing.(TH) degree from the Technical University of Darmstadt, Darmstadt, Germany, in 1985, and the Dr.-Ing. (Ph.D.) degree from Fern-Universität, Hagen, Germany, in 1991.

Since 1994, he has been a Research Engineer with the Microwave Department, Ferdinand-Braun-Institut, Berlin, Germany. His current research interests include electromagnetic simulations, especially microwave packaging emphasizing transitions, e.g., flip chip technologies, BGA submounts, transitions from hollow waveguides to MS, measurement probes (metrology requirements), and calibration sets.



Wolfgang Heinrich (M'84–SM'95–F'09) received the Diploma, Ph.D., and Habilitation degrees from the Technical University of Darmstadt, Darmstadt, Germany.

Since 1993, he has been the Head of the Microwave Department and the Deputy Director with the Ferdinand-Braun-Institut (FBH), Berlin, Germany. Since 2008, he has also been a Professor with the Technical University of Berlin, Berlin. He has authored or co-authored more than 350 publications and conference contributions. His current research interests include monolithic microwave integrated circuit (MMIC) design, especially GaN power amplifiers, millimeter-wave (mm-wave) integrated circuits, and electromagnetic simulation.

Dr. Heinrich serves for the microwave community in various functions. He was the President of the European Microwave Association (EuMA) from 2010 to 2018.